Reduced statistical fluctuations of the position of an object partitioning in two its environment

Eugenio DelRe, Paolo Di Porto, Stefano Di Sabatino, and Bruno Crosignani

Citation: AIP Conference Proceedings **1411**, 7 (2011); doi: 10.1063/1.3665228
View online: http://dx.doi.org/10.1063/1.3665228
View Table of Contents: http://scitation.aip.org/content/aip/proceeding/aipcp/1411?ver=pdfcov
Published by the AIP Publishing

Reduced statistical fluctuations of the position of an object partitioning in two its environment

Eugenio DelRe*, Paolo Di Porto†, Stefano Di Sabatino* and Bruno Crosignani**

*Department of Electrical and Information Engineering, University of L'Aquila, 67100 L'Aquila, Italy and IPCF-CNR, University of Rome Sapienza, 00185 Rome, Italy
†IPCF-CNR, University of Rome Sapienza, 00185 Rome, Italy
**Applied Physics Department, California Institute of Technology, Pasadena CA 91125, USA

Abstract.
Through hard-disk simulations and theoretical considerations on the movement of an object that partitions a microtubule filled with small particles, we find that the vibrations typical of thermal equilibrium are reached after a time that increases exponentially with the number of particles involved. The result is a mechanism capable of breaching, on accessible time scales, the ergodic constraints in nano-scale systems.

Keywords: Out-of-equilibrium physics, hard-sphere simulations, adiabatic piston
PACS: 05.70.-a,31.15.xv,05.70.Ln

INTRODUCTION

Objects that are so small as to feel the single collisions of the tiny agitated molecules that make up their hosting liquid or gas, move randomly about their equilibrium position [1]. The understanding of these movements rests on the so-called ergodic hypothesis which leads to the fundamental $1/\sqrt{N}$ relative statistical noise law for significant quantities, where N is the number of molecules that interact with the object [2]. Small systems with a small value of N have a noise-dominated trajectory [3]. We here demonstrate that ergodicity, and its $1/\sqrt{N}$ noise limit, is to all practical purposes violated and replaced by a considerably lower noise limit for "partitioning" micro-objects, i.e., that separate in two their small and agitated hosting environment. We show the effect in a simple situation where the object slides inside a microtubule. The reduced stochastic vibration breaches statistical limits and forms a paradigm for ultrasensitive instruments, such as would be used in storing information in ever smaller memory chips [4], for the design and operation of non-Brownian deterministic microscale mechanical motors, and in the interpretation of specific nanometric cellular machinery, such as molecular motors that slide minute proteins along nanometric microtubules [5, 6, 7, 8]. It also forms a paradigm for the modeling and numerical simulation of non-ergodic behavior directly from first principle molecular dynamics, establishing a fundamentally new perspective on the nature of complex phenomena.

Second Law of Thermodynamics: Status and Challenges
AIP Conf. Proc. 1411, 7-26 (2011); doi: 10.1063/1.3665228

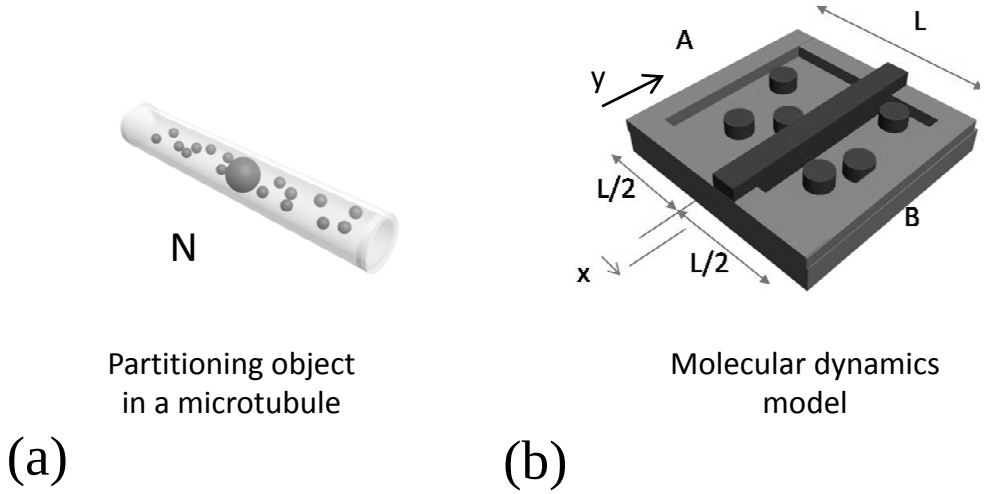

FIGURE 1. (a) General layout of an object (large sphere) sliding along a microtubule filled with smaller particles (small spheres). (b) Molecular dynamics scheme.

MODEL SYSTEM

Objects at small scales are at the confluence of physical sciences, molecular engineering, and biology, and their behavior holds the key both to innovative man-made devices and to the understanding of living systems. A great challenge at these scales is the understanding of the most simple of all questions we can formulate: How do things move? Is there a level of deterministic precision at these scales, or does the erratic motion of the single parts, i.e., micro-springs, cogs, and levers, caused by the inevitable agitation of molecules in the environment, always dominate, so that the universal mechanism for directed operation rests on rectified Brownian motion? [9]

A microscopic partitioning particle

Our investigation refers to the situation illustrated in Fig.(1)a, that is an object (the large sphere) that slides along a microtubule and is in contact with N microscopic agitated particles (the small spheres). The geometry reproduces one of the basic paradigms for cellular micromotion, where microtubules are thought to act as "conveyer belts" for

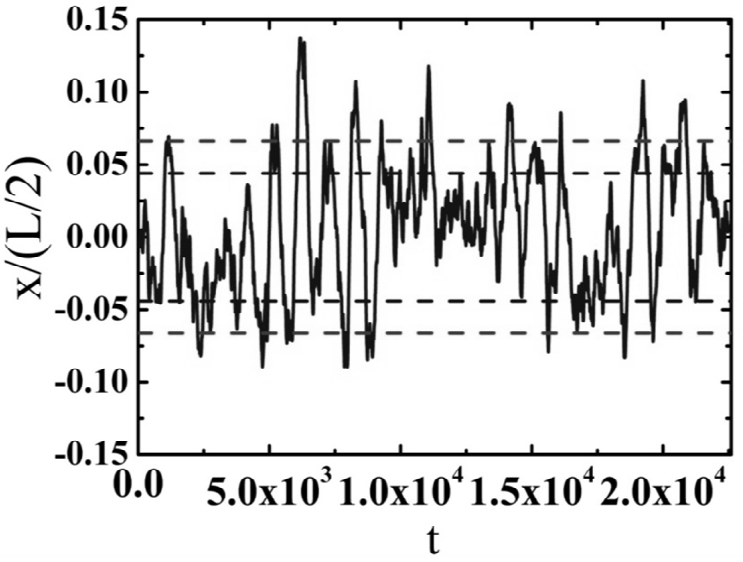

FIGURE 2. Example of the object trajectory $x(t)/(L/2)$ (full curve) for $N = 200$, $m = 1$, and $M = 20$. Superimposed are the values of $x/(L/2) = \pm 1/\sqrt{N}$ and $x/(L/2) = \pm 1/\sqrt{2N}$ (the two sets of dashed lines, corrected for the effect of the finite covolume (see Detailed description and derivations)).

kinesis [9, 10, 11, 12]. Our basic finding is that, when the object partitions the microtubule in two, it suffers statistical noise well below the $1/\sqrt{N}$ limit associated with the ergodic hypothesis. Molecular dynamics (MD) simulations are implemented on the flat system illustrated in Fig.(1)b. The partitioning object is therefore a rigid segment of mass M (the wall) and side L that slides along one axis (the x axis) of a square $L \times L$ container (the microtubule). The opposing agitated molecular environments are N rigid disks of mass m (the small disks) contained in the microtubule and separated into two closed compartments, A and B, each containing $N/2$ disks, by the sliding particle. These form the reservoirs for the object's motion [9].

NUMERICAL SIMULATIONS

The dynamics are calculated using standard algorithms (see Detailed description and derivations), and a typical trajectory of the object is shown in Fig.(2) (full curve). Analyzing the stochastic process, we find the remarkable result that the system undergoes an initial dynamic phase that settles to a value for the fluctuations in position $\langle x^2 \rangle^{1/2}/(L/2) \simeq 0.045$ (squares in Fig.(3)), considerably lower that the value

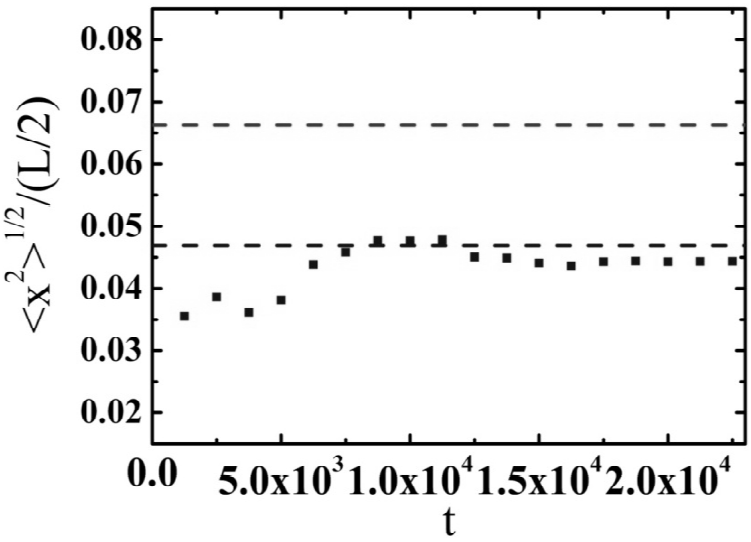

FIGURE 3. Fluctuations are evaluated through the corresponding value of $\langle x^2\rangle^{1/2}/(L/2) = ((1/t)\int_0^t (x(t')/(L/2))^2 dt')^{1/2}$ (root-mean square of the object position), which saturates to the value 0.045 (squares) considerably lower than the ergodic expectation $1/\sqrt{N} \simeq 0.071$ (0.066 taking into account the finite covolume, top dashed line).

$1/\sqrt{N} \simeq 0.071$ ($N = 200$, dashed line in Fig.(2) and Fig.(3)). (see Detailed description and derivations)

The values of $\langle x^2\rangle^{1/2}/(L/2)$ in this long-lasting initial phase (the first "plateau") are systematically lower than $1/\sqrt{N}$ for different values of N and for a wide range of inspected values of systems parameters, with the only constraint that the topology is left unchanged, i.e., the object partitions the environment in two.

THEORETICAL CONSIDERATIONS

The reduced fluctuations stem from an unexpected but intuitive alteration in the molecule-molecule interaction caused by the partitioning object (the underlying "topology"). According to general ergodic theory, the $1/\sqrt{N}$ law (Eq.(8) in Detailed description and derivations) expresses the notion that each particle can have any kinetic energy from 0 to E_0, where E_0 is the *entire* energy of the isolated system. In distinction to standard Brownian motion, in the present case the object partitions the system in two. For a molecule in section A to occupy a high energy phase-space region close to

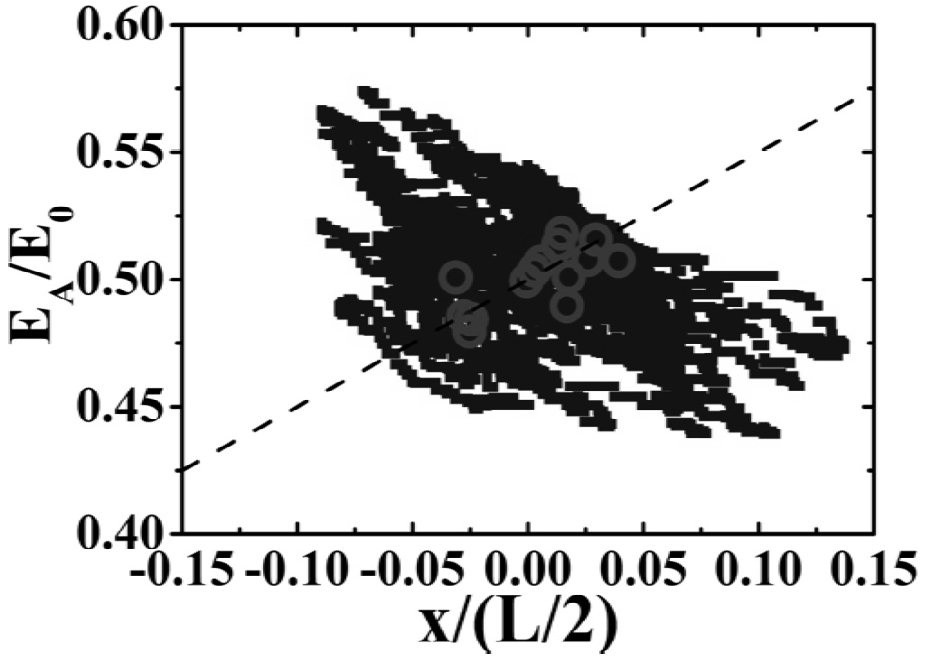

FIGURE 4. Phase-space analysis of $x(t)$. Plot of $E_A(t)/E_0$ ($E_A(t)$ is the total energy in section A) versus $x(t)/(L/2)$ (squares) shows that for average values (on Δt =1250, circles) an approximate and loose validity of an "equation of state" holds (dashed line, see Detailed description and derivations).

E_0, it is necessary that the object transfers to the particle a macroscopic quantity of energy collected from the particles in section B, which are not directly in contact with the particle in A. This implies highly improbable events for which the object collides with a macroscopic portion of the particles in B in a time interval in which it does not undergo collisions with any particle in A. More precisely, the time to reach ergodicity can be estimated as that required for a relative energy fluctuation, from one section to the other, of the order of $1/\sqrt{N/2}$, to occur. This allows enough events to occur so as to build up a significant probability distribution. This requires a $\sqrt{N/2}$-particle event, i.e., a sequence of $\sqrt{N/2}$ collisions occurring on the object from only one of the two sections, and hence a time $2\sqrt{N/2}t_p$, where t_p is the characteristic thermalization time for each separate section. This means that the system is governed by a many-particle effect, and that for any reasonable experimentally available observation time the entire possible phase-space of each particle can never be practically spanned, even for relatively small values of N. The consequence is that, for all practical time scales, vibrations are observed to follow a sub-ergodic behavior, i.e., the

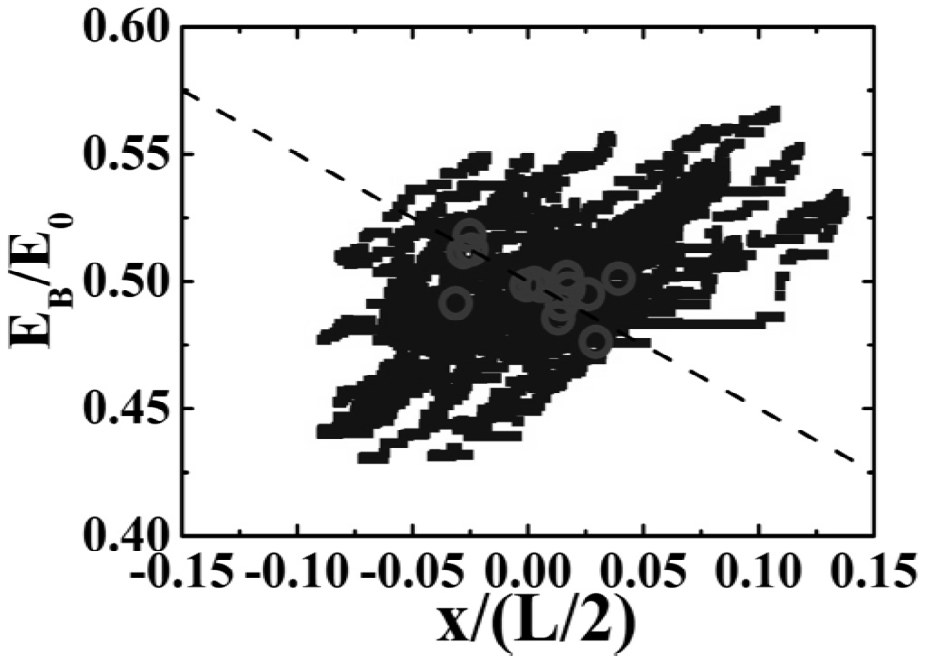

FIGURE 5. Same analysis as previous figure for $E_B(t)/E_0$ (where correspondingly $E_B(t)$ is the total energy of section B).

$$\frac{\langle x^2 \rangle^{1/2}}{(L/2)} = \frac{1}{\sqrt{2N}} \tag{1}$$

prediction, lower dashed line in Fig.(2) and Fig.(8) (see Eq.(14) in Detailed description and derivations). The subergodic behavior can be associated to the approximate validity of an equation of state for sections A (Fig.(4)) and B (Fig.(5)) (see Detailed description and derivations, Eq.(9) and Eq.(10)).

Extending this theory to the general case in which molecules have n quadratic terms in their energy, we have the new general law governing the micro-object's vibrations (see Detailed description and derivations)

$$\frac{\langle x^2 \rangle^{1/2}}{(L/2)} = \frac{1}{\sqrt{\frac{(2+n)N}{2}}}. \tag{2}$$

This means that molecules with more degrees of freedom and a consequent higher value of n will induce a stronger fluctuation reduction. For example, considering a full three-dimensional system extension of the model in Fig.(1)b, we expect reduced fluctuation with

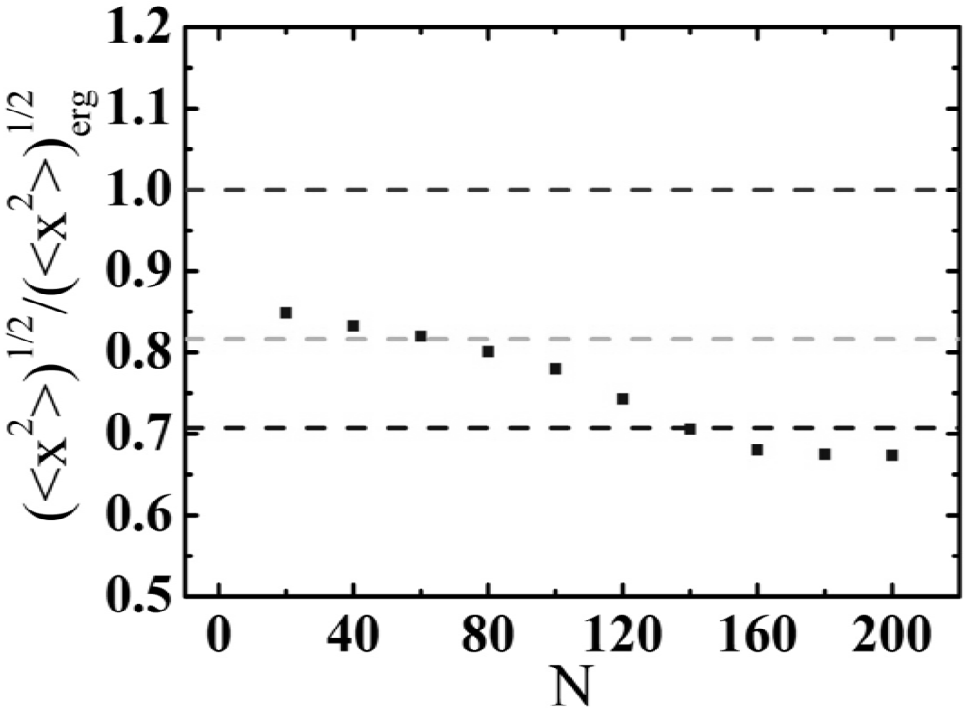

FIGURE 6. Comparison of MD results (squares) to the ergodic prediction of Eq.(8) (top dashed line) and the non-ergodic prediction of Eq.(2) for different values of N, central dashed line for $n = 1$ and bottom dashed line for $n = 2$.

$$\frac{\langle x^2\rangle^{1/2}}{(L/2)} = \frac{1}{\sqrt{5N/2}}. \tag{3}$$

Eq.(2) also describes the transition from $n = 1$ (top dashed line in Fig.(6)) to $n = 2$ (lower dashed line in Fig.(6)) observed in the MD results: for the smaller values of N the reduced scattering between the molecules compared to the scattering off the object renders velocity randomization along y ineffective, so that in this case the kinetic degrees of freedom along the y axis cease to be involved in the reduction of phase-space ($n = 1$).

BREAKDOWN OF ERGODICITY AND LONG-TIME DYNAMICS

For limited values of N the breakdown of ergodicity can be directly observed, by immensely expanding the duration of the MD simulation. This is practically impossible for reasonably large values of N. For the tractable case of $N = 200$, using an event-driven MD (see for example [13]), we are able to span the entire phase space by increasing the time window by more than 6 orders of magnitude with respect to the

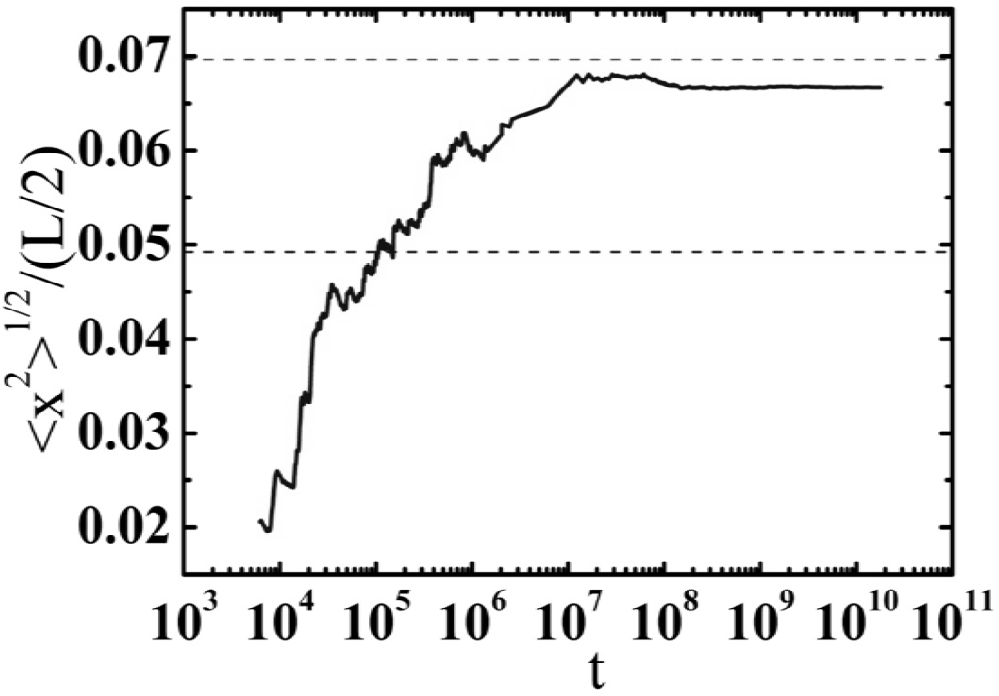

FIGURE 7. A self-similar and ever slower approach to equilibrium. The full curve represents the evolution of $\langle x^2 \rangle^{1/2}/(L/2)$ for a sample in the conditions of the run of Fig.(2) (N=200, M=20). The first region below the lower dashed line (the $n = 2$ prediction of Eq.(2)) is where the condition of practical equilibrium is reached and violates the $1/\sqrt{N}$ law. Here only the probable molecule-molecule interaction events in the separate sections/partitions are active (arrows in the intrapartition rendering of Fig.(8)). The second region above the lower dashed line is so long that even the increasingly improbable events involving energy/information transfer through the object (arrows in the interpartition rendering of Fig.(8)) partake in the dynamics, leading to the ergodic prediction (top dashed line). Note that the exponential-like growth is observed for a logarithmic scale, meaning that the nature of the process has no specific time scale (see Detailed description and derivations). The succession of plateaus in the growth identifies a hierarchy of improbable events that begin to partake in the fluctuations, leading the system ever more slowly towards ergodicity.

observed first asymptotic-like behavior of Fig.(2). The results are reported in Fig.(7) and have a number of remarkable features. The first is that the approach to the ergodic limit of $\langle x^2 \rangle^{1/2}/(L/2)$ occurs with an ever increasing slowness (see the exponential like approach in the logarithmic time scale in Fig.(7)). The second is that plateaus are manifest even in the logarithmic scale, so that each one can be considered a practical asymptotic behavior, and the time evolution displays a characteristic self-similarity that indicates a scaleless time evolution (see Fig.(9), Fig.(10), Fig.(11)). The finding fits well into our understanding of the dynamics, that appears to be scaleless in time (see Detailed description and derivations). Quantitatively, if we assume room temperature

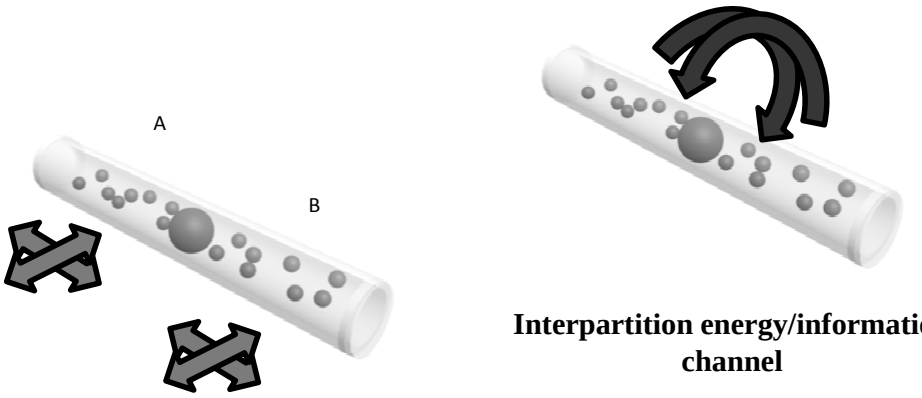

FIGURE 8. Schematic rendering of processes involved in the different regimes of Fig.(7).

hydrogen atoms ($m \simeq 1.66 \cdot 10^{-27}$kg, $E_0/2N \simeq 2 \cdot 10^{-21}$J) in a square $L = 10$ nm container, the sub-ergodic fluctuations (first plateau in Fig.(2)b) are reached on a scale of 0.1 ns, remain fixed to the basic correction of Eq.(2) ($n = 2$) on the scale of 1 ns, and grow at an ever slower rate, to reach the ergodic fluctuations on a scale of 0.1 ms (Fig.(7)). We underline that non-ergodic behavior associated with the continuum of different time scales emerges directly from first principle dynamics, a fact that suggests a more profound interpretation of complexity as arising from the presence of partitioning objects.

GENERALIZATIONS AND APPLICATIONS

The reduction in vibrations associated to the value of n in Eq.(2) is dependent on the spatial scale of system. For example, as systems grow from nanometric to micrometric scales, the vibrating object representing the micro-gadget will cease to be a single rigid body and its parts will participate in the microagitation, progressively washing out the phase-space reduction (see Detailed description and derivations). We underline that the present investigation can be extended to the case in which the two sections do not contain the same number of particles (i.e., $N_A \neq N_B$), so that the equilibrium position along the

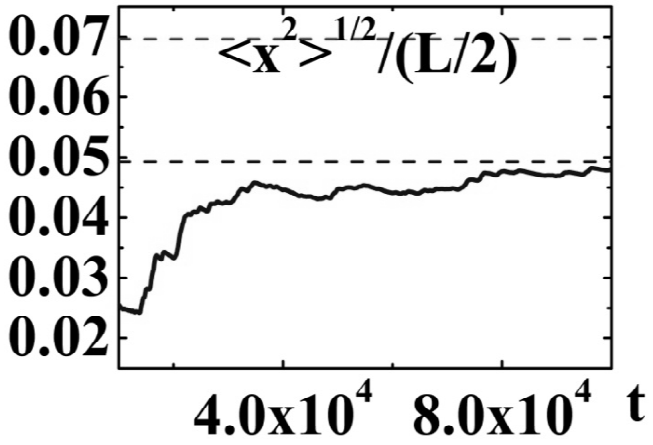

FIGURE 9. The scaleless nature of the effect is highlighted by the self-similarity observed at different time scales in a linear time plot. Case of short time dynamics.

tubule is determined by the ratio of N_A/N_B (see Supplementary Information). Reduced fluctuations will also occur when an external force contributes to keep the object at the equilibrium position (see Supplementary Information).

A partitioning object represents a self-incorporated and efficient noise reduction paradigm that allows to preserve small freely sliding things from heat disorder and hence to tolerate a stochastic environment [14]. It addresses the question of how to locally reduce vibrations and realize linear and rotational motion in a controlled and reversible fashion, such as in the form of strokes. It is of central importance to formulate new ideas on locomotion, muscle contraction, particle separation, and micro-pumping, along with new schemes to interface standard mechanics with the whole realm of microscopic elements, i.e., for micro-tweezers, ultrasensitive sensors, and artificial biosensors, and can also suggest models for biomachines that seem to require some form of deterministic mechanical behavior, such as in DNA transcription. The universality of the effect is well highlighted by its applicability to many different fields of science. For example, the object in the tubule allows the storage of more information bits than would be expected taking into account conventional statistical noise (see Supplementary Information).

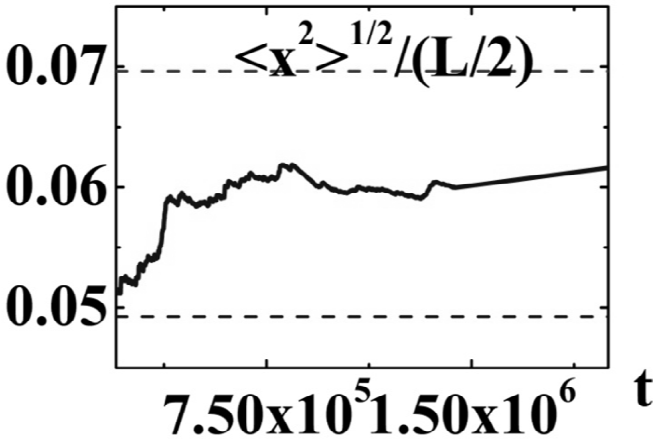

FIGURE 10. Scale-less nature of the effect. Intermediate time dynamics.

DETAILED DESCRIPTION AND DERIVATIONS

Molecular dynamics simulations are carried out through standard techniques for rigid disks. For extended simulations leading to the ergodic limit, event-driven techniques are implemented. The physical value of the time intervals is determined by fixing the value of L, m, and E_0. The $\langle x\rangle^{1/2}_{ergodic}/(L/2) = 1/\sqrt{N}$ limit is calculated taking into account the full phase-space of the system. The sub-ergodic limit $\langle x\rangle^{1/2}/(L/2) = 1/\sqrt{2N}$ is calculated taking into account the reduced phase-space implied by the loose validity of an equation of state for each of the two sections separately. This reduction is generalized by extending this constraint to molecules with n kinetic degrees of freedom. Predicted fluctuations are corrected to take into account the effect of covolume by altering the available phase-space. The progressive fading of the sub-ergodic effect for increasing object size is argued on the basis of the role of its internal degrees of freedom. Scaleless time evolution is derived by the approximate fitting of values of $\langle x^2\rangle^{1/2}/(L/2)$ on long-time scales (Fig.(2)a) to an exponential growth law in the logarithmic scale.

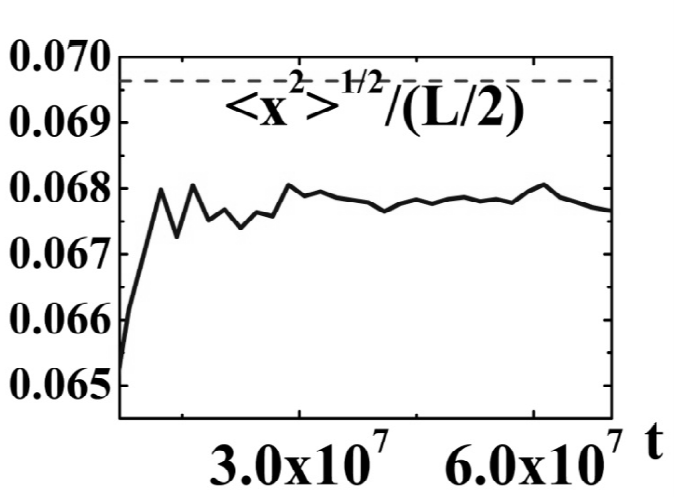

FIGURE 11. Scale-less nature of the effect. Long time dynamics.

Molecular dynamics

The numerical approach to fluctuations follows the lines of rigid-disks in piston-like systems [15]. At $t = 0$ the $N/2$ particles in each section are distributed on an appropriate grid in the available space and are attributed a random initial velocity from a Maxwell distribution compatible with an equal total energy in the sections, $E_A(t = 0) = E_B(t = 0) = E_0/2$. The object starts from the central position (dividing the square in two) $x(t = 0) = 0$ with initial zero velocity. The specific simulations consider the dynamics on a 4000×4000 spatial lattice, with each microscopic molecule of diameter $\sigma = 80$ lattice spacings, and initial Maxwell distribution taken with $(\langle v_x^2 \rangle)^{1/2} = (\langle v_y^2 \rangle)^{1/2} = 5$ lattice spacings per unit time. Establishing the value of L, m, and E_0 determines the unit of time through the relationship

$$\frac{1}{2} m \langle v_x^2 \rangle = \frac{E_0}{2N}. \tag{4}$$

Ergodic prediction: the $1/\sqrt{N}$ law

General considerations allow us to formulate an understanding of the reduced vibration in the object and its relationship to topology. The ergodic evaluation of the fluctuations of the object position considers the $(N+1)$ dimensional Γ-phase space, each point of which corresponds to a given value of the x_i coordinate for each of the N molecules (the disks) and of object x. The volume $d\Gamma$ corresponding to an object position in the range x and $x+dx$ depends on x through the constraint on the particle positions imposed by the object itself: particles in section A are confined in the region $(-L/2,x)$ and the B particles in $(x,L/2)$. Accordingly,

$$d\Gamma = \left(\frac{L}{2}+x\right)^{N/2}\left(\frac{L}{2}-x\right)^{N/2}dx = \left(\frac{L}{2}\right)^{N}\left(1-4\frac{x^2}{L^2}\right)^{N/2}dx, \tag{5}$$

i.e., in the limit $N \gg 1$ and dropping the inessential constant $(L/2)^N$,

$$d\Gamma = \exp\left(-\frac{2Nx^2}{L^2}\right)dx. \tag{6}$$

If, at equilibrium, each member of the system ensemble is equally likely to be in any one of the various possible microstates (ergodic hypothesis), the time-independent probability density $p(x)$ of the object being in the range x and $x+dx$ is proportional to the corresponding phase-space volume, that is

$$p(x) = \sqrt{\frac{2N}{\pi L^2}}\exp\left(-\frac{2Nx^2}{L^2}\right), \tag{7}$$

so that

$$\frac{\langle x^2\rangle^{1/2}_{ergodic}}{(L/2)} = \frac{1}{\sqrt{N}}. \tag{8}$$

Sub-ergodic prediction

The entire phase-space that leads to the ergodic Eq.(8) will be fully spanned when even improbable events that involve an $N/2$ particle collision with the object have occurred, i.e., on a time scale $\sim 2^{N/2}t_p$, where t_p is the characteristic thermalization time for each section. Hence, on experimentally available times, the object will fluctuate on the basis of a partial set of dynamical events in which the improbable collisions are absent. In Fig.(4) we compare the values of $E_A(t)$ (and in Fig.(5) $E_B(t)$) with the object position $x(t)$ (squares) for the case of the dynamics reported in Fig.(2). Comparing the averaged values of $\langle E_A(t)\rangle$ ($\langle E_B(t)\rangle$) and $\langle x(t)\rangle$ along the trajectory indicates that there exists an effective averaged constraint between E_A (and E_B) and $x(t)$ that must be taken into account. For example, in Fig.(4) and Fig.(5) we show the averaged positions for time intervals of Δt=1250 (circles). These loosely lie on the lines (dashed in the figures) for which

$$\frac{E_A}{E_0} = \frac{1}{2}\left(\frac{x}{(L/2)}\right) + \frac{1}{2} \tag{9}$$

and

$$\frac{E_B}{E_0} = -\frac{1}{2}\left(\frac{x}{(L/2)}\right) + \frac{1}{2}. \tag{10}$$

This implies an average validity of a direct proportionality between the volume of each section (i.e., for A, $L(x+L/2)$, and for B, $L(-x+L/2)$) and the energy there contained. For macroscopic systems, this corresponds to a movement of the object in conditions in which the pressures in the two sections are equal and constant (i.e. $p_A = p_B$) [16, 17].

This constraint, even though loose, now affects the previous reasoning leading to Eq.(7). On experimentally achievable time scales, the energy of the single particles in A and B is approximately correlated to the position x of the object, its maximum value being now proportional to $(L/2+x)$ for the particles in A, and to $(L/2-x)$ in B. This modifies the achievable Γ in that the maximum value of particle momentum p_x and p_y, for each particle, scales with $(L/2+x)^{1/2}$ in A and $(L/2-x)^{1/2}$ in B. The new constrained motion will suffer a partially ergodic dynamic associated with the volume

$$d\Gamma = \left(\frac{L}{2}+x\right)^N \left(\frac{L}{2}-x\right)^N dx = \left(\frac{L}{2}\right)^{2N} \left(1-\frac{4x^2}{L^2}\right)^N dx, \tag{11}$$

i.e., in the limit $N \gg 1$ and once again dropping the inessential constant $(L/2)^{2N}$,

$$d\Gamma = \exp\left(-\frac{4Nx^2}{L^2}\right) dx. \tag{12}$$

Retracing the steps of the ergodic calculation, if, at the quasi-equilibrium, each member of the system ensemble is equally likely to be in any one of the various possible microstates (partial ergodic hypothesis), the time-independent probability density $p(x)$ of the object being in the range x and $x+dx$ is proportional to the corresponding phase-space volume, that is

$$p(x) = \sqrt{\frac{4N}{\pi L^2}} \exp\left(-\frac{4Nx^2}{L^2}\right), \tag{13}$$

so that the fluctuations are reduced by a factor $1/\sqrt{2}$

$$\frac{\langle x^2\rangle^{1/2}}{(L/2)} = \frac{1}{\sqrt{2N}}. \tag{14}$$

General reduction of vibrations

Each kinetic degree of freedom that thermalizes in each section separately becomes correlated to x and introduces a factor to the phase space $(L/2+x)^{1/2}$, for each particle in A,

and $(L/2-x)^{1/2}$, for each particle in B. This leads to Eq.(14) when the kinetic degrees of freedom are $n=2$ (disks sliding in a plane), and to Eq.(2) for the general case of arbitrary n. Intuitively, vibrations in the object position, which should be solely associated with fluctuations in the volume of the two sections, here follow the fluctuations in energy.

Covolume

For relatively large values of N the finite volume occupied by the molecules, even though leading to changes in predictions that are far lower than those associated to the partitioning effect, must be taken into account in the theory. Considering the relative covolume

$$\varepsilon = \frac{(N\pi\sigma^2/8)}{(L^2/2)}, \tag{15}$$

the finite size of the disks entails that the spatial component of the phase space volume for a single disk reads $L(L/2+x)-L(L/2)\varepsilon$ (for section A), and $L(L/2-x)-L(L/2)\varepsilon$ (for section B). All equations, and hence Eq.(2) and Eq.(14), are approximately modified by substituting L with $L(1-\varepsilon)$ in the actual predictions. For example, for the observations in Fig.(2), $\varepsilon \simeq 0.06$.

Macroscopic system

As the size of the system increases, the assumption that the partitioning object acts as a single rigid body becomes growingly less adherent, to the point that the object will actually transmit energy between the two sections through standard single collisions with its own internal degrees of freedom and the molecules. The mechanism leading to the sub-ergodic reduced fluctuations is no longer efficient for macroscopic systems, and is masked by the standard ergodic fluctuations of Eq.(8). To grasp the physics underlying this transition from microscopic physics to the macroscopic case, we can consider the case in which the partitioning object conducts heat, that is, it is no longer a single rigid body (a "diathermal" object). Referring to the model system represented in Fig.(1), the large sphere of panel (a) and the separating wall of panel (b) are now excellent heat conductors. We proceed to analyse the fluctuations of the partitioning object around the central equilibrium position ($x=0$) without directly making use of the phase-space analysis. We begin by observing that the assumption of excellent heat conductivity implies that under reasonable conditions, a constant temperature T_0 is continuously restored in both sections A and B. This means that the corresponding pressures $p_A(x)$ and $p_B(x)$ are given by

$$p_A(x) = \frac{Nk_BT_0}{2S(L/2+x)} \tag{16}$$

$$p_B(x) = \frac{Nk_BT_0}{2S(L/2-x)} \tag{17}$$

where S is the transverse section area. As a consequence, the deterministic component $F(x)$ of the force exerted by the "gas" on the piston is

$$F(x) = \frac{Nk_BT_0}{2(L/2+x)} - \frac{Nk_BT_0}{2(L/2-x)}. \tag{18}$$

If we now assume that $|x| \ll L/2$ (an assumption that we must check self-consistently a posteriori), Eq.(18) reads

$$F(x) = -\frac{Nk_BT_0}{(L/2)^2}x. \tag{19}$$

Therefore, the object of mass M feels both the thermal bath at the temperature T_0 and the harmonic potential

$$V(x) = \frac{Nk_BT_0}{2(L/2)^2}x^2. \tag{20}$$

The random object motion around $x = 0$ can now be dealt with in the frame of the theory of Brownian motion of a body in an assigned deterministic field of force [1]. This is accomplished by solving the Langevin-like equation

$$\frac{d^2x}{dt^2} = -\beta\frac{dx}{dt} + A(t) + \frac{F(x)}{M}, \tag{21}$$

which reads, in our case (see Eq.(18)),

$$\frac{d^2x}{dt^2} + \beta\frac{dx}{dt} + \omega^2 x = A(t), \tag{22}$$

where

$$\omega = \left[\frac{Nk_BT_0}{M(L/2)^2}\right]^{1/2}, \tag{23}$$

$A(t)$ is the fluctuating Langevin acceleration, and $-\beta\frac{dx}{dt}$ is the frictional term (the friction coefficient β could be readily evaluated by considering the kinematics of a slowly moving object hitting fast molecules [16], although its value is inessential in the present frame). As a particular result of the considered Langevin approach, we obtain (see [1])

$$\lim_{t\to\infty}\left\langle x^2(t)\right\rangle = \frac{k_BT_0}{m\omega^2}, \tag{24}$$

i.e., with the help of Eq.(23),

$$\lim_{t\to\infty}\frac{\left\langle x^2(t)\right\rangle^{1/2}}{L/2} = \frac{1}{\sqrt{N}}, \tag{25}$$

in agreement with the ergodic result of Eq.(8), based on the homogeneous spanning of the allowed phase-space. As a further relevant result, we observe that the way in which

$\left\langle x^2(t)\right\rangle$ tends to its asymptotic values (Eq.(24)) corresponds to a regular exponential-like behavior (see Eqs.(214,217) of Ref.([1])). This sheds light on the peculiar nature of microscopic partitioning object as compared to the macroscopic version (adiabatic object as opposed to a diathermal object). While in the latter case the asymototic value of the fluctuation amplitude Eq.(25) is attained through an ordinary exponential time behavior, in the former case the same final value is reached in a different way. A number of temporal platforms are present, during which the non-heat-conducting object performs stationary position fluctuations. Their amplitudes are smaller than the asymptotic ergodic value of Eq.(25), and this corresponds to the peculiar sub-ergodic behavior of the system considered in the present paper.

Scaleless time evolution

Inspection of the long-time evolution of $\left\langle x^2\right\rangle^{1/2}/(L/2)$ in Fig.(7) suggests that the approach to the ergodic limit occurs according to an exponential-like law in the logarithmic plot. This means that

$$\frac{\left\langle x^2\right\rangle^{1/2}}{(L/2)} = \left[\frac{\left\langle x^2\right\rangle^{1/2}_{ergodic}}{(L/2)}\right][1-\exp(-\alpha z)] \tag{26}$$

with $z=\log(t)$, so that the approach to equilibrium would follow a $(1-t^{-\alpha})$ law. A power law of this kind has no characteristic time scale: this fits well into the physical picture that a whole family of very different time scales, i.e., the hierarchy of effects associated to single-particle collisions that scale with t_p, two-particle collisions that scale with $2^1 t_p$, three-particle collisions that scale with $2^2 t_p$, and so on, contributes to the process after the first plateau has been reached at t_p.

SUPPLEMENTARY INFORMATION

Arbitrary equilibrium position

Simple symmetry considerations indicate that the equilibrium position of the partitioning object when the number of molecules in section A and section B is different, i.e., $N_A \neq N_B$, is at a distance $LN_A/(N_A+N_B)$ from the fixed wall of section A. Thus, changing the ratio N_A/N_B allows an arbitrary choice of its average position. Retracing the procedures that lead to Eq.(8) and Eq.(14), these are generalized into

$$\frac{\left\langle x^2\right\rangle^{1/2}_{ergodic}}{L/2} = \frac{2}{N\sqrt{1/N_A+1/N_B}} \tag{27}$$

and

$$\frac{\langle x^2\rangle^{1/2}}{L/2} = \frac{\sqrt{2}}{N\sqrt{1/N_A + 1/N_B}} \tag{28}$$

where $N = N_A + N_B$.

External potential binding the object

When ergodicity holds, the connection between fluctuations and a binding potential $V(x)$ can be evaluated through the Maxwell-Boltzmann statistics, that is, introducing a probability function

$$p(x) \propto e^{-\frac{V(x)}{k_B T}}, \tag{29}$$

where k_B is the Boltzmann constant. Since $p(x)$ must coincide with the expression in Eq.(7), then

$$V(x) = \left(\frac{1}{2}\right)\frac{N k_B T x^2}{(L/2)^2}, \tag{30}$$

an expression that can also be deduced by considering the effect of the different pressures in the two sections, for $x \neq 0$. If an external potential is added, for example a harmonic

$$V_e = \left(\frac{1}{2}\right) k x^2, \tag{31}$$

where k is a constant, the resulting potential $V(x) + V_e(x)$ leads to

$$\frac{\langle x^2\rangle^{1/2}_{ergodic}}{L/2} = \left[\frac{k_B T}{k_B T N + k(L/2)^2}\right]. \tag{32}$$

In the first plateau (results in Fig.(3)), our previous results indicate that a form of ergodicity holds separately for the two sections with the substitution of N with $2N$, so that

$$\frac{\langle x^2\rangle^{1/2}}{L/2} = \left[\frac{k_B T}{2k_B T N + k(L/2)^2}\right]. \tag{33}$$

Once again, reduced fluctuations are predicted.

Enhanced information storage

The microtubule in Fig.(1)a can be used to store information in the position of the object along the tubule, using $N_A \neq N_B$. The question is how much information can be stored in the site and how this quantity diminishes as N decreases and wiggling

takes over. To quantify the information that can at best be stored in the microtubule, we calculate how many different positions of equilibrium can be distinguished, i.e, are separated by a distance $\langle x^2 \rangle^{1/2}$. At each specific equilibrium position

$$X = \frac{LN_A}{(N_A + N_B)} \tag{34}$$

(measured from the top of the tubule in section A), the $\langle x^2 \rangle^{1/2}$ in the ergodic case of Eq.(27) is expressed as function of X and the number of distinguishable states is

$$n_{bits}^{ergodic} \simeq \int_0^L dX \sqrt{\frac{N}{[X(L-X)]}} = \pi\sqrt{N}. \tag{35}$$

In the non-ergodic case, this number is increased to

$$n_{bits} = \sqrt{2} n_{bits}^{ergodic}. \tag{36}$$

The register can therefore store numbers that are exponentially larger than in the ergodic case as N increases.

ACKNOWLEDGMENTS

The research leading to these results has received funding from the Italian Ministry of Research (MIUR) through the "Futuro in Ricerca" FIRB-grant PHOCOS - RBFR08E7VA. Partial funding was received through the SMARTCONFOCAL project of the Regione Lazio. Correspondence and requests for materials should be addressed to E.D.R. (email: eugenio.delre@univaq.it.)

REFERENCES

1. S. Chandrasekhar, "Stochastic problems in physics and astronomy", Rev. Mod. Phys. 15, 1-89 (1943)
2. H.B. Callen, "Thermodynamics and an introduction to thermostatics", Second Ed. (Wiley, New York, 1985)
3. E. Schroedinger, "What is Life ?" (Cambridge University Press, Cambridge, 1944)
4. M. H. Lankhorst, B. W. Ketelaars, and R. A. Wolters, "Minimum voltage for threshold switching in nanoscale phase-change memory", Nature Materials 4, 347-352 (2005)
5. R. D. Astumian, "Thermodynamics and kinetics of a Brownian motor", Science 276, 917 (1997)
6. F. Julicher, A. Ajdari, and J. Prost, "Modeling molecular motors", Rev. Mod. Phys. 69, 1269 (1997)
7. P. Reimann, "Brownian motors: noisy transport far from equilibrium", Phys. Rep. 361, 57 (2002)
8. W.R. Browne, B.L. Feringa, "Synthetic molecular machines at work - automotive mechanics in nanoland", Nature Nanotechnology 1, 25 (2006)
9. R. D. Astumian and P. Hanggi, "Brownian motors", Physics Today Nov. 2002, 33-39 (2002)
10. F. Julicher, J. Prost, "Cooperative molecular motors", Phys. Rev. Lett. 75, 2618-2621 (1995)
11. D. Odde, "Diffusion inside microtubules", Eur. Biophys. J. 27, 514-520 (1998)
12. G. Bao and S. Suresh, "Cell and molecular mechanics of biological materials", Nature Materials 2, 715-725 (2003)
13. D. C. Rapaport,"The event scheduling problem in molecular dynamic simulation", J. Comput. Phys. 34, 184-201 (1980).

14. H. Linke, M. T. Downton, and M. J. Zuckermann, "Performance characteristics of Brownian motors", Chaos 15, 026111 (2005)
15. J.A. White, F.L. Roman, A. Gonzalez, and S. Velasco, "The adiabatic piston at equilibrium: Spectral analysis and time-correlation function", Europhys. Lett. 59, 479-485 (2002)
16. B. Crosignani, P. Di Porto, and M. Segev, "Approach to thermal equilibrium in a system with adiabatic constraints", Am. J. Phys. 64, 610 (1996).
17. P. Castiglione, M. Falcioni, A. Lesne, and A. Vulpiani, "Chaos and Coarse Graining in Statistical Mechanics" (Cambridge University Press, Cambridge, 2008), page 203.